Naccache, R., Mazhorova, A., Clerici, M. , Piccoli, R., Khorashad, L. K., Govorov, A. O., Razzari, L., Vetrone, F. and Morandotti, R. (2017) Terahertz thermometry: combining hyperspectral imaging and temperature mapping at terahertz frequencies. Laser and Photonics Reviews, 11(5), 1600342.

There may be differences between this version and the published version. You are advised to consult the publisher's version if you wish to cite from it.

This is the peer reviewed version of the following article: Naccache, R., Mazhorova, A., Clerici, M. , Piccoli, R., Khorashad, L. K., Govorov, A. O., Razzari, L., Vetrone, F. and Morandotti, R. (2017) Terahertz thermometry: combining hyperspectral imaging and temperature mapping at terahertz frequencies. Laser and Photonics Reviews, 11(5), 1600342, which has been published in final form at http://dx.doi.org/10.1002/lpor.201600342. This article may be used for non-commercial purposes in accordance with Wiley Terms and Conditions for Self-Archiving.

http://eprints.gla.ac.uk/144369/

Deposited on: 21 August 2017

Enlighten – Research publications by members of the University of Glasgow
http://eprints.gla.ac.uk

Terahertz Thermometry: Combining Hyperspectral Imaging and Temperature Mapping at Terahertz Frequencies

Rafik Naccache,* Anna Mazhorova, Matteo Clerici, Riccardo Piccoli, Larousse Khosravi Khorashad, Alexander O. Govorov, Luca Razzari, Fiorenzo Vetrone,* and Roberto Morandotti*

The accurate and non-invasive determination of multiple physical parameters, with well-defined spatial resolution, is crucial for applications in manufacturing, chemistry, medicine and biology. Specifically, the ability to simultaneously measure both temperature and spectral signatures is still experimentally unavailable. To this end, we propose a mapping technique for biological systems, which exploits a linear correlation between terahertz wave reflectivity and temperature, and allows to spatially and spectrally resolve thermal distributions. This method is applied to a model biological system in two relevant cases where in one example, nanoplasmonic-induced photothermal effects are imaged gaining new insights into collective heating phenomena. In the second example, we demonstrate a joint thermal-hyperspectral imaging approach to chemically map the presence of a model drug formulation and simultaneously investigate its thermal stability in our biological system. This concept can be easily extended and widely applied to all materials that demonstrate a measurable change in their dielectric properties.

1. Introduction

Temperature is a physical parameter of fundamental importance, as it dictates the properties of materials, the rates of chemical reactions, or even the health of biological systems. In spite of recent and impressive advancements,[1,2] non-invasive temperature measurements continue to pose a challenge, considering that simple approaches rely on physical contact with the sample, *e.g.,* thermocouple probes or catheters, which are only practical for surface sensing and may induce discomfort, damage and/or contamination.[3] This can be mitigated by using non-contact temperature-sensing techniques, including infrared (IR) thermography and optical thermometry.[4–13] The former detects radiation in the wavelength range of 3–14 μm. It is temperature-sensitive since the amount of IR radiation emitted by an object increases with temperature and can be mea-sured in a non-destructive way. On the other hand, a partic-ular branch of optical thermometry, namely nanothermome-try, relies on changes in the luminescent properties of nano-sized probes and can be used to extract local temperatures with

R. Naccache, A. Mazhorova, M. Clerici, R. Piccoli, L. Razzari, F. Vetrone, R. Morandotti
Institut National de la Recherche Scientifique (INRS), Centre Énergie, Matériaux et Télécommunications (EMT)
Université du Québec
Varennes, QC, Canada, J3X 1S2
E-mail: rafik.naccache@concordia.ca; vetrone@emt.inrs.ca; morandotti@emt.inrs.ca

M. Clerici
School of Engineering
University of Glasgow
Glasgow, United Kingdom, G12 8LT

L. Khosravi Khorashad, A. O. Govorov
Department of Physics and Astronomy
Clippinger Research Labs
Ohio University
Athens, Ohio, United States of America, 45701

F. Vetrone
Centre for Self-Assembled Chemical Structures
McGill University
Montreal, QC, Canada, H3A 2K6

R. Naccache
Presently at: Department of Chemistry and Biochemistry
Concordia University
Montreal, QC, Canada, H4B 1R6

F. Vetrone
Institute of Fundamental and Frontier Sciences
University of Electronic Science and Technology of China
Chengdu 610054, China

R. Morandotti
Institute of Fundamental and Frontier Sciences
University of Electronic Science and Technology of China
Chengdu 610054, China

R. Morandotti
National Research University of Information Technologies
Mechanics and Optics
St Petersburg, Russia

A. O. Govorov
Institute of Fundamental and Frontier Sciences
University of Electronic Science and Technology of China
Chengdu 610054, China

sub-micrometric spatial resolution. Such techniques have been investigated in areas spanning micro/nano-electronics, integrated photonics and biomedicine.[7] While both methods are highly sensitive due to recent advances in materials synthesis and optical characterization, they either require the physical injection of luminescent nanoprobes and/or cannot be easily used to measure the temperature when a sample is obstructed or beyond-line-of-sight. Based on the properties of terahertz (THz) radiation, we demonstrate a temperature sensing technique that addresses these shortcomings, and which we use to investigate photothermal events in a biological model system.

Terahertz covers the portion of the electromagnetic spectrum between 0.1 to 10 THz (3 mm - 30 μm in wavelength); it is non-ionizing and thus will not perturb the physical or chemical integrity of a material.[14–17] THz radiation can be generated using several approaches including optical rectification of ultrashort pulses,[18,19] as in our case; however, recent developments on small footprint continuous wave lasers will allow for the generation of THz radiation using more compact sources.[20] Typical spatial resolutions are on the order of the wavelength as dictated by diffraction effects; however, THz has the potential to offer information at significantly smaller scales given that recently, THz-based sub-wavelength imaging techniques have been developed.[21–23] More importantly, THz radiation is highly sensitive to water,[24–26] which has an inherently central role in multiple biological processes.

In this work, we capitalize on the unique properties of THz radiation to demonstrate the possibility of temperature sensing in aqueous media, where the sensitivity of THz waves to moisture content exhibits a strong temperature dependence. By harnessing THz waves, we are able to investigate an important and relatively unexplored phenomenon at the nanoscale, namely collective heating in biosystems, where a significant increase in heating effects can occur in ensembles of plasmonic nanomaterials due to cumulative effects in a large ensemble of heated plasmonic gold nanorods (GNRs). Moreover, we demonstrate the ability of simultaneously generating both thermal and hyperspectral maps in our biological system and apply our versatile approach to two relevant situations: (i) the localized temperature increase induced by photothermal heating of injected plasmonic GNRs, and (ii) the thermally-dependent chemical mapping of an injected model drug formulation.

2. Experimental Setup

THz pulses were generated through optical rectification of femtosecond pulses delivered by a Ti:Sapphire regenerative amplifier (Spectra-Physics Spitfire). The source emits a train of 120 fs pulses with the optical spectrum centered at $\lambda = 800$ nm, at a repetition rate of 1 kHz. The laser beam is divided by a dielectric beamsplitter into two parts: the pump and the probe beams. The pump laser excites a 1-mm thick (<110> cut) second-order nonlinear Zinc Telluride (ZnTe), which emits a sub-picosecond THz pulse. The generated THz radiation is focused on the sample by means of a pair of parabolic reflectors. A prismatic 90° reflector separates the beam reflected by the sample from the incident beam. The reflected beam is collected and focused onto the detector (also a 1-mm thick, <110> cut ZnTe crystal) by means of two parabolic mirrors. Terahertz detection is performed with a standard electro-optical sampling technique. It is a time-gated electric field measurement routinely used to record the temporal profile of THz signals. A short 800 nm probe pulse is overlapped to the THz field inside a second-order nonlinear crystal. The phase of the probe pulse is modulated by the THz field and recorded via a balanced polarisation detection. The recorded phase modulation is proportional to the THz electric field sampled by the short pulse. In our experiment, the balance detection signal is acquired through a lock-in amplifier, locked to the modulation signal imposed on the pump laser beam by an optical chopper (not shown in **Figure 1**a). In order to maximize the signal, the optical chopper is driven by a sub-harmonic of the laser train signal. Specifically, the phase-locked chopper is driven at 500 Hz, that is, half of the laser repetition rate.

THz imaging was carried out at room temperature and humidity (20°C, ~35-40 % RH) where THz time-resolved traces were recorded for each spatial coordinate of a 2-D sample using a raster scanning technique. Images were obtained by scanning the porcine skin sample through the THz beam focus, while collecting the reflected THz signal by means of off-axis parabolic mirrors (Figure 1a). The porcine skin sample was mounted on a 3-D motorized translation stage (2 dimensions, x and y, for image scanning across the sample, and a third one along the focal position of the THz beam). The imaging resolution was limited by the numerical aperture of our setup (NA~ 0.45) to nearly 330 μm at 1 THz. Images were sampled at 8/mm spatial frequency.

Ibuprofen bulk drug (99%), in powder form and polyethylene glycol (PEG $M_n = 1000$) were purchased from Sigma-Aldrich and used without any further modifications. The Ibuprofen powder was compressed into a pellet, for THz analysis, using a manual Carver press operated at 10,000 psi for 30 seconds. The model drug formulation was prepared by combining 2:1 (w/w) Ibuprofen bulk with PEG 1000 and mixing them with a spatula. The formulation was then used without further modification. Spectroscopic analysis and imaging of the Ibuprofen bulk drug and PEG 1000 (separately and/or as a mixture) were carried out as previously highlighted.

3. Results and Discussion

In order to develop our teramometer (THz-thermometer), we first characterized the temperature-dependent reflectivity of the THz waves in water using a reflection geometry setup. To achieve this, we experimentally established the function relating the THz reflectivity to the temperature, i.e. the calibration curve of the teramometer. To this end, a volume of water is precisely heated in the temperature range of 25–60°C while monitoring the sample reflectivity at THz frequencies via electro-optical sampling. This temperature range is chosen due to its biological relevance. The water is confined in a metallic cell equipped with a low-density polyethylene (LDPE) polymer window that is transparent to THz radiation. We note that a visible increase of the reflectivity of water can be directly appreciated by comparing the time-resolved electric field traces of the signal reflected from the sample at 25 and 60°C (inset in Figure S1a). The THz reflectivity is measured and correlated to the sample temperature (Figure S1a), resulting in a linear trend with a correlation coefficient (R^2) of ~0.99.

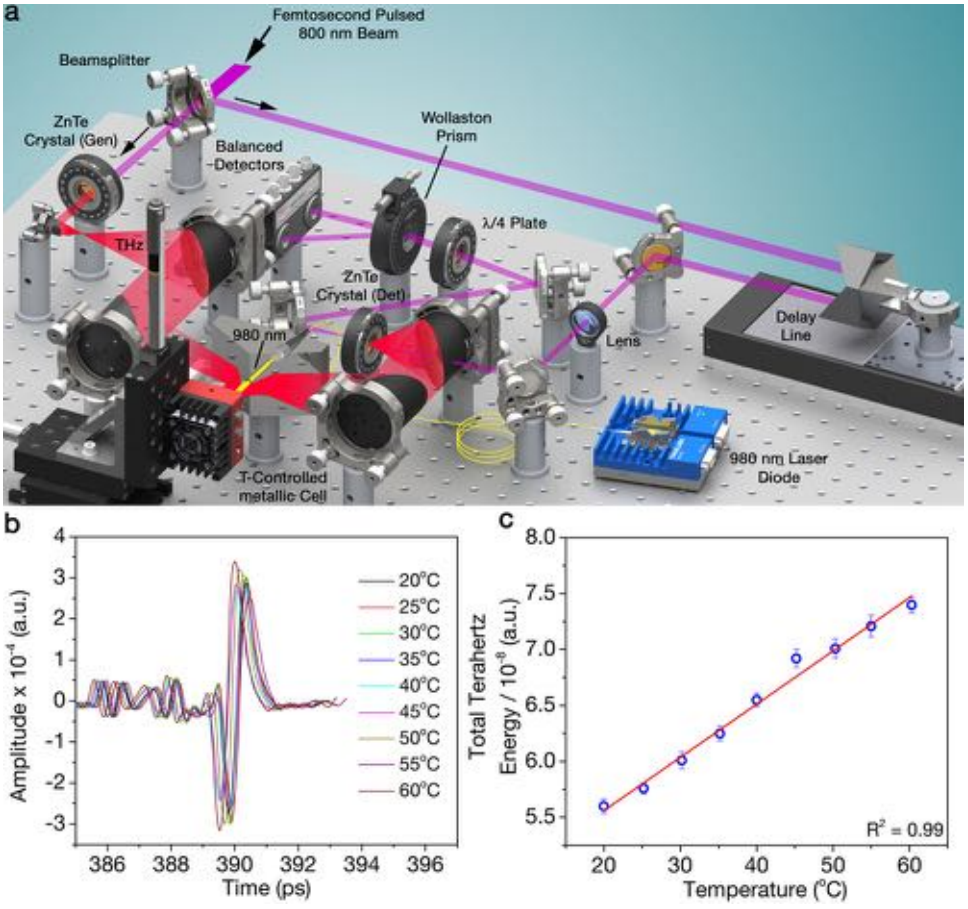

Figure 1. Experimental THz-TDS spectroscopy setup and THz-dependent temperature calibration. (A) Experimental THz-TDS setup in reflection mode. The 980 nm NIR beam, used to plasmonically heat gold nanorods, enters an opening in the center of the polished aluminum prism reaching the sample holder. (B) The THz time trace of the porcine skin, injected with 10 μL of GNR dispersion, is recorded following controlled heating in the metallic sample holder. The sample is allowed to stabilize at each temperature for 10 minutes prior to acquisition of the THz trace with all analyses repeated in triplicate. (C) Linear change in the total THz energy in the range of 20–60°C, for porcine skin injected with 10 μL of GNR dispersion.

The value of the reflectivity has been calculated by integrating the square of the THz electric field measurements over a 5 ps window. The measured change in reflectivity can be associated to a change in the water refractive index, which varies by up to 8% in the temperature interval between 20–60°C at 1 THz, and is in agreement with previous reports performed at similar temperatures and for similar frequencies.[27,28] In the considered case, the water layer is thicker than the penetration depth of the THz radiation (0.1 mm, as shown in the supplementary information). Therefore, the response of the THz detector to the temperature is independent of the thickness of the sample.

Local hyperthermia, the confined increase of temperature above normal bodily values, is currently under investigation in cancer therapy.[29–33] Its proper implementation requires both contactless real-time thermal sensing and the ability to gather diagnostic information at the target, which might be beyond-line-of-sight for optical detectors. To mimic a hyperthermia-like environment, we synthesized and optically excited an ensemble of GNRs (inset in Figure S1), which exhibited a mean particle size of 45.5 ± 9.2 nm in length and 8.5 ± 3.5 nm in width. The aspect ratio (length:width) was calculated to be 5.35:1. The GNRs were tailored to feature a strong surface plasmon resonance[34] centered at ~1020 nm (100 nm FWHM, see Figure S1) that is efficiently excited using a near infrared 980 nm diode laser. The resulting strong absorption, at this wavelength, induces an increase of temperature in the host, a process known as plasmonic, or photothermal, heating.[35,36] In order to calibrate our approach, we injected GNRs in the biological model, namely porcine skin, and we varied the temperature of a sample injected with 10 μL of aqueous GNRs, (in the range of 20–60°C) by means of an external heating plate. Then, using a THz time domain spectroscopy setup (THz-TDS)[37,38] configured in reflection geometry (Figure 1a), we recorded the THz-reflectivity dependence as a function of temperature (Figure 1b-c) showing a linear correlation. From the linear regression model, the calibration process leads to a temperature sensitivity limited to 1.5 °C within the temperature range spanning 20–60 °C. For the photothermal heating experiment, a NIR laser diode was used to optically excite the injected GNRs in the sample without the use of an external heating plate. At a power density of 50 W/cm^2, we found that the local temperature increased by 21.3 ± 1.5°C (see Supplementary Materials) attributed to the efficient excitation of the GNRs by the 980 nm

laser beam. We note that in a living tissue (basal temperature of 37°C), this increment leads to a peak temperature of 58.3°C, *i.e.* sufficient for inducing cell death.[39] As a reference, we illuminated a sample where only pure water was injected, without GNRs, noting that at the same power density, the local temperature increased by 4.2 ± 0.9°C only (as estimated from an average of three different measurements, Figure S2).

We demonstrate the thermal imaging capabilities of the proposed technique by raster scanning our sample, injected with GNRs, through the THz beam focus, while recording the reflected THz signal. Here, we perform THz-reflectivity scans over a 6×7 mm^2 area (**Figure 2**a), in the absence of plasmonic heating (experimental reference image), and we then excite the sample with 980 nm light at various power densities. In order to match living tissue conditions, we maintained the skin at a temperature of 37°C. Thermal images were obtained by subtracting the reference map from those recorded with plasmonic heating, and by applying the temperature calibration described in Figure 1c. At low excitation power densities of the GNRs, ≤ 17 W/cm^2, we observed a moderate temperature rise of 5.0 ± 1.5°C (Figure 2b). In contrast, at 38 W/cm^2 (Figure 2c), we recorded a peak temperature rise of 15.5 ± 1.5 °C at the centre of the GNRs injection site (covering $\sim 2 \times 2$ mm^2) showing that the skin sample is locally heated to 52.5 ± 1.5 °C. The proposed scheme relies on a differential measurement, and is therefore robust against the environment noise including power and temperature fluctuations of the surroundings. We further investigated the potential for beyond-line-of-sight thermal imaging on a fresh injection site (Figure 2d). The sample was covered with a double-layered medical gauze prior to THz thermal imaging (Figure 2e). The recorded temperature was 52.0 ± 1.5 °C (Figure 2f), which is in excellent quantitative agreement with the unobstructed sample illuminated with the same power density of 38 W/cm^2. The excitation beam is able to efficiently excite the obstructed and subcutaneously injected GNRs. We observe that the scattering from the gauze layers appears to mask the irregularities of the skin, leading to a more uniform background relative to an unobstructed sample.

It is interesting to compare the maximum temperature in our system and the temperature at the surface of a single GNR that is thermally isolated from all the other nano-heaters. By using the model presented in the Supplementary Materials, we find that the ratio of these temperatures, in the porcine skin model, can be expressed as follows,

$$\frac{\Delta T_{\text{collective, max}}\,(r=0)}{\Delta T_{\text{single GNR}}\,(\textit{at surface of GNR})} = \frac{51.2^{\circ}\text{C}}{0.026^{\circ}\text{C}} \sim 2000, \qquad (1)$$

We observed a particularly strong collective heating effect. This is typical for the plasmonic nano-heater collections composed of a large number of nanoparticles. Approximately $\sim 10^8$ GNRs were estimated to contribute to the collective temperature in our system. Physically, this heat accumulation effect is very strong because of the long-range character of the heat fluxes created by single GNRs.

In what follows, we demonstrate, for the first time, collective heating in a biological system and we also find that the results are in excellent agreement with our theoretical predictions. The strong heating effects measured in Figure 2g-h are quite significant considering that one GNR can only increase its surface temperature by small amounts equivalent to less than 0.026 °C (see Figure S5). The observed thermal effects must therefore be attributed to the joint action of millions of GNRs that can collectively induce a much larger change in temperature. The collective heating effects can be explained by two main mechanisms:[40,41] (i) the accumulative effect due to the addition of heat fluxes generated by individual GNRs and (ii) the Coulomb interaction effect considering that GNRs interact through plasmon-enhanced electric fields. Thus, the recorded rise in temperature will depend on the inter-GNR distance, GNR arrangements, and the particle-particle interactions. In our system, mechanism (i) is dominant leading to a strong photoheating effect. At excitation power densities of 38 W/cm^2 and by taking into account our experimental parameters, we theoretically predict a temperature increase of 16°C relative to the background (in very good agreement with the measured values presented in Figures 2c and 2f). This represents a $\sim$2000 fold increase relative to the maximum value expected for the case of a single non-interacting GNR (Figure S5 and S7). In order to obtain the shape and parameters for the spatial region of the injected GNRs, we first characterize the injection depth of the GNRs in the porcine skin using scanning electron microscopy (SEM) as depicted in Figure S8. We find the injection to be centered at $\sim$0.26 mm below the surface, spanning 1.20 mm in length and 0.36 mm in depth (and up to 0.08 mm below the surface). Based on SEM imaging, the GNR injection site is clearly distinguishable from the remainder of the skin sample, which does not bear any GNRs. The appearance of the rods can be described as the "bumpy" features within the perimeter of the injection site. These features were further characterized using electron dispersive spectroscopy (EDS) (inset of Figure S8) where the EDS spectrum confirms the presence of GNRs (area shaded in red), as evidenced by the characteristic gold peak at 2.12 keV. Using these results, we can reproduce the experimental temperatures using a realistic model based on the Maxwell's and thermal transfer equations, where we incorporate GNRs as a continuous absorbing region. In our hybrid bio-system, the estimated number of GNRs contributing to the collective temperature amounts to $\sim 10^8$ particles. Figure 2i shows the distribution of temperature in the modeled system. In the center of the image, we observe a maximum calculated temperature rise of 16°C. At a distance of 0.5 to 1 mm from the center, the temperature rise is $\sim$10°C. At distances of 1.5 and 2 mm, the rise amounts to 7°C and 2°C, respectively. Qualitatively, the heat accumulation effect is very strong because of the long-range character of the heat fluxes created by single nanoscale sources - in good agreement with our experimental results. This is evidenced in Figure 2i where the modeled heat distribution (taken across the white dashed lines in Figure 2h) is compared to its experimental counterpart. Therefore, the results obtained in our theoretical model are in good agreement with our experimental findings. In our samples, a large number of GNRs generate collectively relatively large excess temperatures under relatively weak illumination. This collective heating regime provides an excellent opportunity to controllably increase the temperature of a macroscopic region of tissue without thermal damage to cells and surroundings.

Teramometry offers the unprecedented ability to concomitantly and independently retrieve thermal, spectral and spatial information. To demonstrate this important point, we prepared a model drug formulation (2:1 Ibuprofen /Polyethylene Glycol,

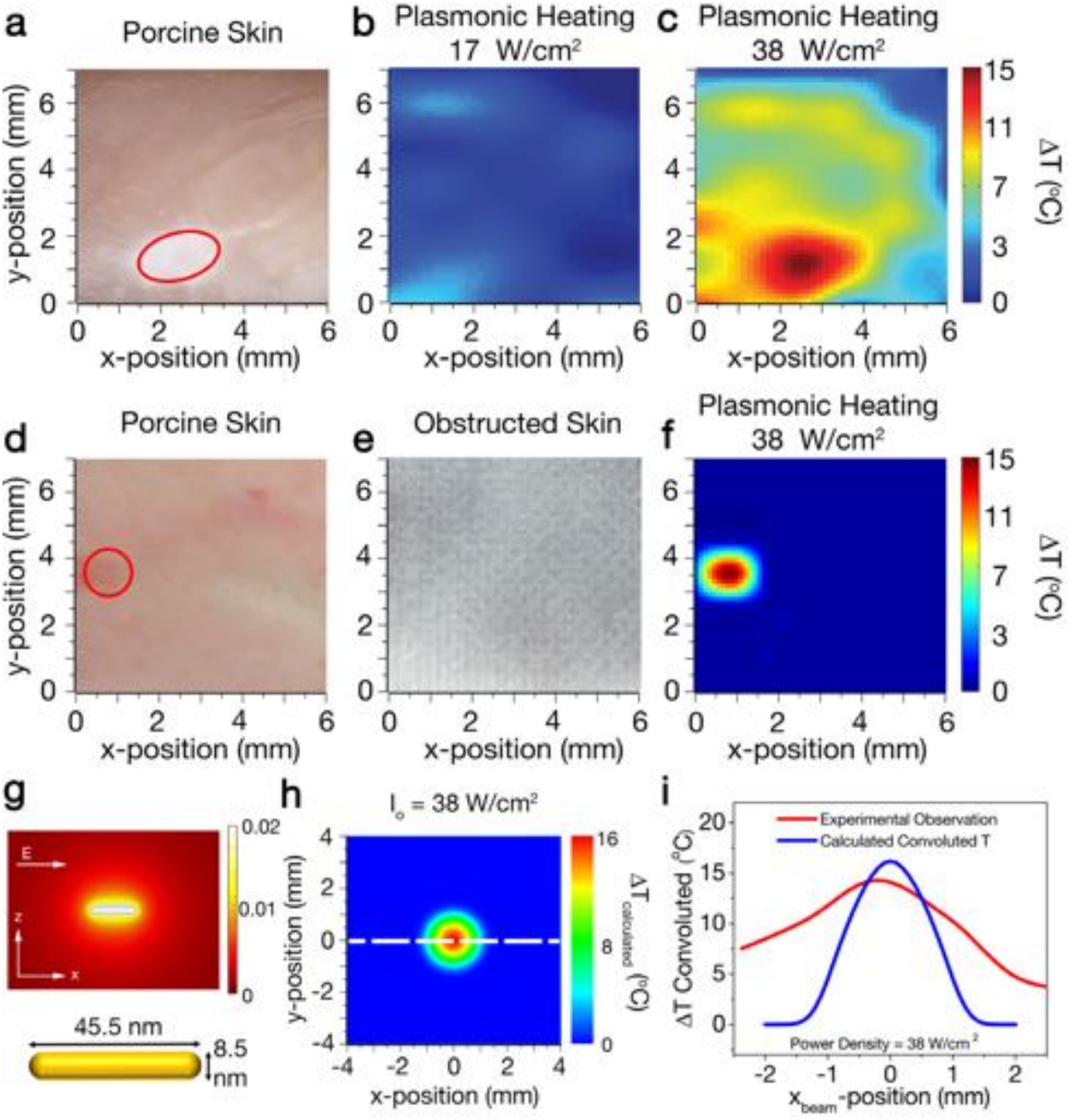

Figure 2. Teramometry for thermal imaging. (A) Digital photograph of the actual sample of porcine skin injected with GNRs. The red ellipse marks the injection site. The skin is heated to a reference temperature of 37°C, and a reference temperature map is recorded (not shown). Thermal image maps (b and c) following plasmonic photoexcitation of the injected GNRs where the reference is subtracted from the maps of the plasmonically heated samples. By using our previous calibration in Figure 1c, we derive a linear temperature scale used to re-construct the maps. (B) 17 W/cm^2 excitation power density, resulting in no significant increase in temperature at the injection site. (C) 38 W/cm^2 excitation power density, showing a 16 °C localized temperature rise at the injection site, allowing the sample to reach the maximum temperature of ~ 53 °C. (D) Digital photograph of a second sample of porcine skin injected with GNRs. The red circle marks the site of injection. (E) Skin sample wrapped in double layers of medical gauze prior to THz imaging. (F) Corresponding thermal map, recorded under the same experimental conditions of 38 W/cm^2 irradiation. The temperature measured in this experiment was 52 °C, which is similar to the maximum temperature achieved for the unobstructed sample (see Figure 2c). (G) Top: a calculated map showing the spatial distribution of local temperature created by a single GNR inside a skin under an optical illumination of 38 W/cm^2. Bottom: dimensions of a single GNR with an average length (longitudinal axis) of 45.5 nm and an average width (transverse axis) of 8.5 nm. (H) Calculated map of the "convoluted" temperature of the skin, spanning a range of 16°C. (I) Plot comparing the experimental result versus the calculated "convoluted" temperature taken across the dashed line in Figure 2h.

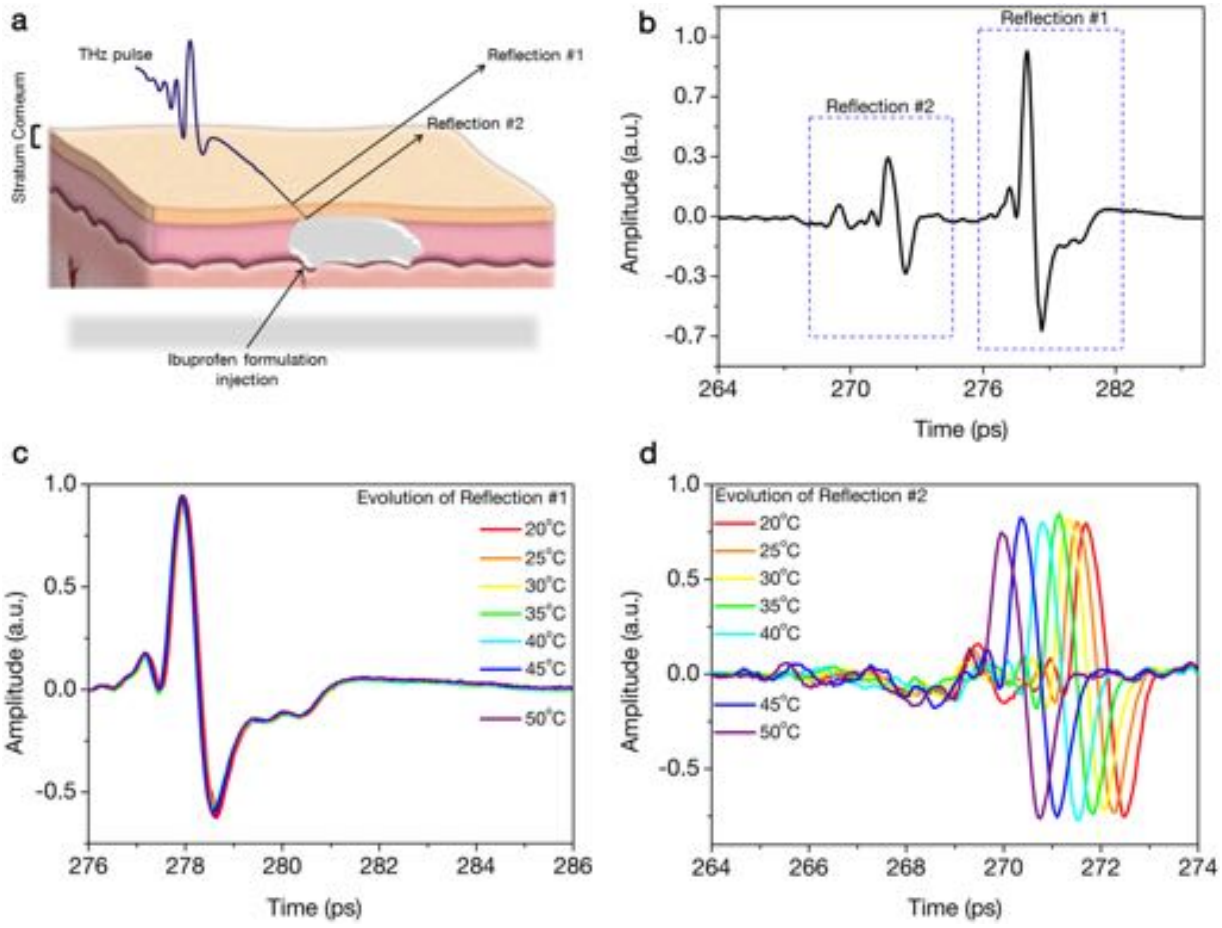

Figure 3. THz interaction with an injected model drug formulation in porcine skin. (A) Digital illustration depicting the main THz reflections in a porcine skin sample injected with the Ibuprofen model formulation. The two distinct reflections from our sample are ascribed to the air/stratum corneum (reflection #1) and the stratum corneum/drug formulation (reflection #2) interfaces, respectively. (B) Temporal profile of the collected THz radiation, in a 20 ps time window, featuring both reflections. (C) Evolution of the THz trace as a function of temperature for reflection #1. (D) Evolution of the THz trace as a function of temperature for reflection #2.

PEG1000, with clear THz signatures). We injected 2 μL of this formulation in the porcine skin tissue (**Figure 3**a) and we then performed THz spectroscopy on the sample, mounted on a heating plate to control its temperature, and observed two distinct reflections (Figure 3b) that can be ascribed to the air/stratum corneum (reflection #1) and the stratum corneum/drug formulation (reflection #2) interfaces. We monitored the evolution of both reflections as a function of temperature (Figures 3c-d). While reflection #1 can be used to extract the temperature of the sample (see Supporting Information), the changes observed for reflection #2 are ideally suited to retrieve the spectral information of the drug formulation.

We show a hyperspectral image (6 × 7 mm^2) of the sample in **Figure 4**a, where the location of the injection is clearly identified by the presence of the two spectral Ibuprofen signatures at 1.04 and 1.27 THz (Figures 4b–c). In Figure 4d, we show the spectral evolution of these two features as a function of the temperature. A significant spectral shift of 0.1 THz was observed for the Ibuprofen signature at 1.04 THz as the temperature increases from 20 to 50°C, which underlines a structural change in the formulation (Figure 4e, black coloured circles). We note a linear trend in the spectral shift up to 37°C followed by a saturation, which corresponds to the melting point of PEG 1000 (37–40°C),[42] representing the transition from the gel to the liquid phase.

Finally, we demonstrate the ability to simultaneously and independently perform temperature mapping and hyperspectral imaging in the same system. To do so, we separately injected our model drug formulation and the GNR colloidal dispersion in the porcine skin tissue (**Figure 5**a). The GNRs injection site was plasmonically heated with a 980 nm laser beam, as previously described. Remarkably, we are able to map both the drug formulation distribution and the local temperature rise, which in this case has a peak value of 9°C (Figures 5b–e).

4. Conclusions

In conclusion, we propose a novel approach to temperature sensing and imaging using THz spectroscopy (teramometry) by taking advantage of the dielectric properties of water, the

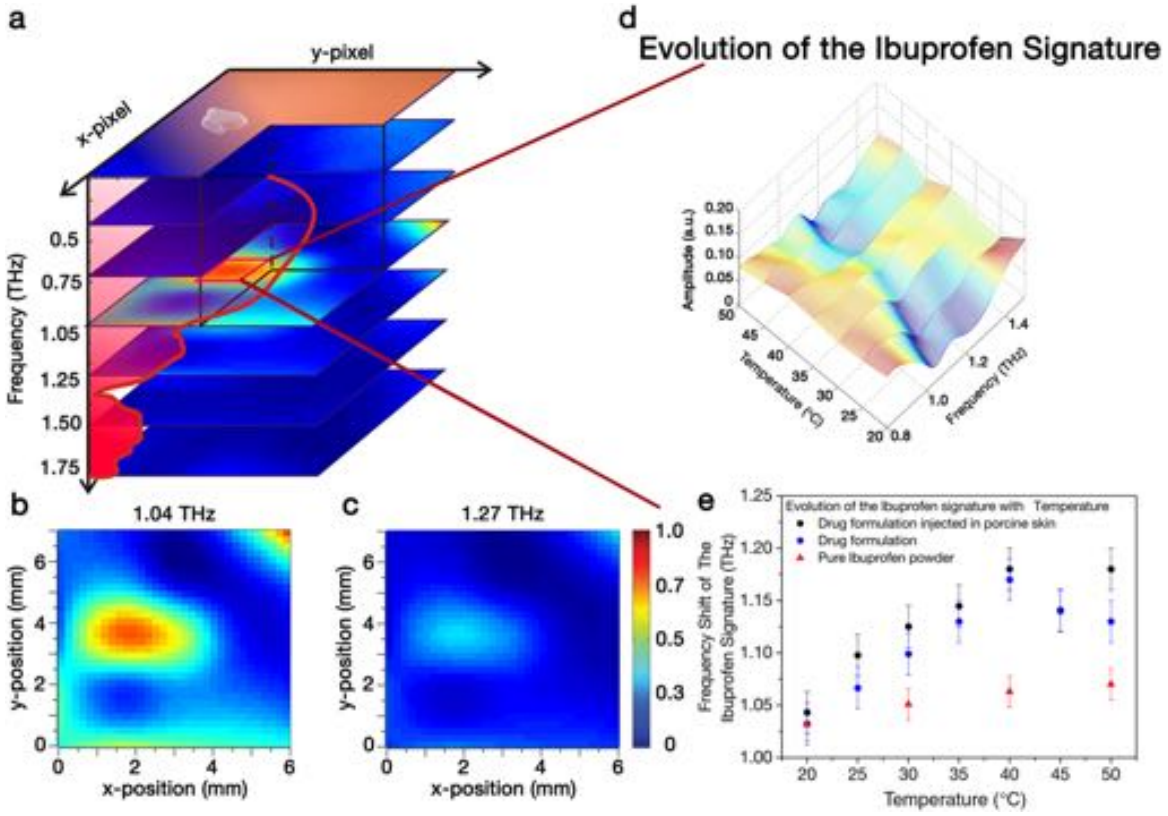

Figure 4. Probing spectroscopic information using Teramometry. (A) Hyperspectral image of the porcine skin injected with 2 μL of the Ibuprofen/PEG 1000 formulation (represented by the white injection spot on the top layer). The three-dimensional image is composed of a set of raster scanning images, recovered at specific THz frequencies. The location of the injection site can be identified by the presence of the Ibuprofen signatures at 1.04 THz and 1.27 THz in the recovered reflected spectrum; Mapping of the injection site using THz raster scanning technique at both (B) 1.04 and (C) 1.27 THz. (D) 3-D plot of the spectral features of the model formulation as a function of frequency and temperature. (E) Spectral shift of the Ibuprofen features vs temperature, in pure Ibuprofen (red triangles), model drug formulation (blue circles) and model formulation injected in the porcine skin (black circles). The red shaded area represents the melting point range of PEG 1000.

most common and significant component of biological systems. It can be foreseen that THz imaging adds further, important advantages: (i) teramometry is independent of the thermal background (providing better S/N ratio), (ii) it offers the possibility to obtain, in the future, additional spectroscopic information and (iii) it opens up the ability to penetrate certain materials such as clothes and bandages. The demonstrated concept can be easily extended and widely applied to all materials that display a measurable change in their dielectric properties. In the framework of temperature imaging, exploiting plasmonic heating using gold nanoparticles allows us to study local changes of temperature in aqueous media and in a biological model system. This approach is quite versatile as it is both contact- and wear-free. Even more importantly, teramometry is a versatile tool that can be used to simultaneously reconstruct the temperature map of a sample and spectroscopically characterize it, in the THz range. This can find important applications in biology and medicine. For example, it can be used in heat-driven therapeutic drug release applications,[43] where for example an organic drug molecule may be tethered to a GNR and selectively released with heat. Our technique will ensure that the target temperature is achieved while maintaining the physical integrity of the drug compound.

Acknowledgements

R.N. is grateful to NSERC for financial support through a Postdoctoral Fellowship, and to Concordia University for Startup funding. M.C. acknowledges the support from the IOF People Programme (Marie Curie Actions) of the European Union's FP7-2012, KOHERENT, GA 299522. A.M. acknowledges support from Mitacs Elevate Postdoctoral Fellowship. F.V., R.M. and L.R. are grateful for financial support from the Natural Sciences and Engineering Research Council (NSERC) of Canada and the Fonds de Recherche du Québec – Nature et Technologies (FRQNT). RM also would like to acknowledge support from the Canadian Institute for Photonic Innovations (CIPI), and The Canada Research Chair Program. R.M. acknowledges additional support by the Government of the Russian Federation through the ITMO Fellowship and Professorship Program (grant 074-U 01) and from the 1000 Talents Sichuan Program in China. L.K.K. and A.O.G. thank the Volkswagen Foundation and the INRS (Canada) for support. R.P. is grateful to FRQNT for financial support through a Postdoctoral Fellowship (PBEEE). We would like to thank Dr. David Naylor from Blue Sky Spectroscopy Inc., Dr. Todd Wilke from Photon Control R&D Ltd., and Dr. Marc Verhaegen from Photon etc. for supporting the research.

The authors would like to thank Mr. D. Iasenza for providing fresh porcine skin samples throughout the course of the research work. They are also grateful to Mr. A. Rovere and J. Xin for work carried out on theoretical simulations with GNRs and Prof. L. Kalman at Concordia University for use of the UV/VIS/NIR spectrometer. The authors would also like to thank Prof. A. Tavarez for enlightening discussions. R.N. and A.M. contributed equally to this work.

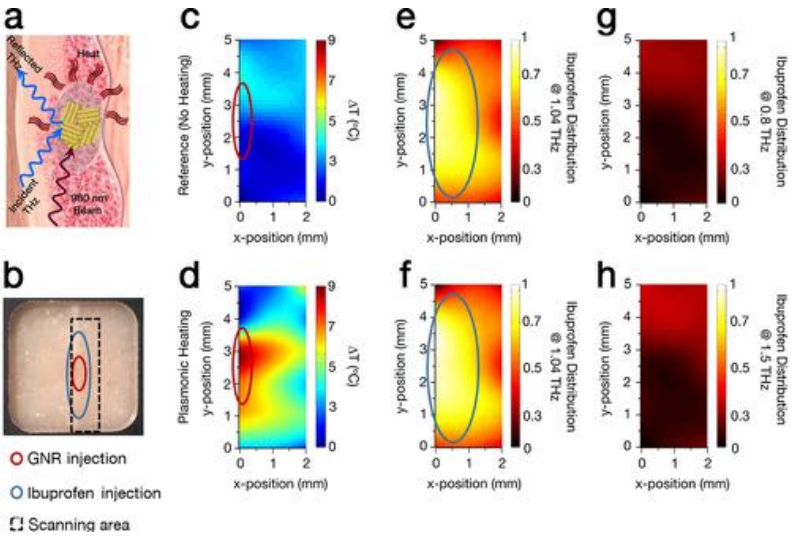

Figure 5. Teramometry for simultaneous and independent thermal and hyperspectral imaging. (A). Digital illustration depicting the porcine skin injected with GNRs and the Ibuprofen/PEG model formulation. The 980 nm beam will optically excite the GNRs that will heat, in turn, the surroundings. Hyperspectral imaging using THz waves was then carried out. (B) Digital photograph of the porcine skin sample injected with both the colloidal GNR dispersion and the model formulation. Due to the shape of the injections, the scanning area was limited to 2 × 5 m m ^{2}. The red ellipse marks the smaller GNR injection site, while the larger blue ellipse marks the model formulation injection site. (C) Reference thermal map obtained in the absence of plasmonic heating. (D) Thermal map obtained under plasmonic heating conditions with an excitation power density of 38 W/cm^2; hyperspectral images of the Ibuprofen distribution at the injection site (E), without, and (F), with, plasmonic heating, when the THz characteristic signature is more evident (1.04 THz). Hyperspectral images of the Ibuprofen distribution at the injection site where Ibuprofen does not show any signature: (G) 0.8 THz, and (H) 1.5 THz.

REFERENCES

[1] W. Weng, J. D. Anstie, T. M. Stace, G. Campbell, F. N. Baynes, A. N. Luiten, *Phys. Rev. Lett.* 2014, **112**, 160801.

[2] P. Neumann, I. Jakobi, F. Dolde, C. Burk, R. Reuter, G. Waldherr, J. Honert, T. Wolf, A. Brunner, J. H. Shim, D. Suter, H. Sumiya, J. Isoya, J. Wrachtrup, *Nano Lett.* 2013, **13**, 2738.

[3] J. L. Robinson, R. F. Seal, D. W. Spady, M. R. Joffres, *J. Pediatr.* 1998, **133**, 553.

[4] G. Gaussorgues, S. Chomet, *Infrared Thermography*, Springer Science & Business Media, Berlin 1994.

[5] M. L. Debasu, D. Ananias, I. Pastoriza-Santos, L. M. Liz-Marzán, J. Rocha, L. D. Carlos, *Adv. Mater.* 2013, **25**, 4868.

[6] F. Vetrone, R. Naccache, A. Zamarrón, A. de la Fuente Juarranz, F. Sanz-Rodríguez, L. Maestro Martinez, E. Martín Rodriguez, D. Jaque, J. García Solé, J. A. Capobianco, *ACS Nano* 2010 **4**, 3254–3258.

[7] D. Jaque, F. Vetrone, *Nanoscale* 2012, **4**, 4301.

[8] G. Kucsko, P. C. Maurer, N. Y. Yao, M. Kubo, H. J. Noh, P. K. Lo, H. Park, M. D. Lukin, *Nature (London, U. K.)* 2013, **500**, 54.

[9] K. Okabe, N. Inada, C. Gota, Y. Harada, T. Funatsu, S. Uchiyama, *Nat. Commun.* 2012, **3**, 705.

[10] O. Katz, E. Small, Y. Bromberg, Y. Silberberg, *Nat. Photon.* 2011, **5**, 372.

[11] I. Calizo, A. A. Balandin, W. Bao, F. Miao, C. N. Lau, *Nano Lett.* 2007, **7**, 2645.

[12] D. Ross, M. Gaitan, L. E. Locascio, *Anal. Chem.* 2001, **73**, 4117.

[13] C. Xie, M. A. Dinno, Y.-Q. Li, *Opt. Lett.* 2002, **27**, 249.

[14] B. Ferguson, X.-C. Zhang, *Nat. Mater.* 2002, **1**, 26.

[15] Y.-S. Lee, *Principles of Terahertz Science and Technology*, Springer, New York 2009.

[16] P. H. Siegel, *IEEE Trans. Microw. Theory* 2002, **50**, 910.

[17] M. Tonouchi, *Nat. Photon.* 2007, **1**, 97.

[18] J.-C. Diels, W. Rudolph, *Ultrashort laser pulse phenomena*, Academic press, 2006.

[19] A. C. Newell, J. V. Moloney, *Nonlinear optics*, Westview Press 1992.

[20] M. Scheller, J. M. Yarborough, J. V. Moloney, M. Fallahi, M. Koch, S. W. Koch, *Opt. Express* 2010, **18**, 27112.

[21] H.-T. Chen, R. Kersting, G. C. Cho, *Appl. Phys. Lett.* 2003, **83**, 3009.

[22] J. Gómez Rivas, C. Schotsch, P. Haring Bolivar, H. Kurz, *Phys. Rev. B: Condens. Matter* 2003, **68**, 201306.

[23] M. Peccianti, M. Clerici, A. Pasquazi, L. Caspani, S. P. Ho, F. Buccheri, J. Ali, A. Busacca, T. Ozaki, R. Morandotti, *IEEE J. Sel. Topics Quantum Electron* 2013, **19**, 8401211.

[24] B. B. Hu, M. C. Nuss, *Opt. Lett.* 1995, **20**, 1716.

[25] D. M. M. Mittleman, R. H. H. Jacobsen, M. C. C. Nuss, *IEEE J. Sel. Top. Quantum Electron.* 1996, **2**, 679.

[26] K. Liu, M. G. Brown, R. J. Saykally, *J. Phys. Chem. A* 1997, **101**, 8995.

[27] C. Rønne, S. R. Keiding, *J. Mol. Liq.* 2002, **101**, 199.

[28] H. R. Zelsmann, *J. Mol. Struct.* 1995, **350**, 95.

[29] X. Huang, S. Neretina, M. A. El-Sayed, *Adv. Mater.* 2009, **21**, 4880.

[30] C. S. S. R. Kumar, F. Mohammad, *Adv. Drug Delivery Rev.* 2011, **63**, 789.

[31] A. Schroeder, D. A. Heller, M. M. Winslow, J. E. Dahlman, G. W. Pratt, R. Langer, T. Jacks, D. G. Anderson, *Nat. Rev. Cancer* 2012, **12**, 39.

[32] S. Mura, J. Nicolas, P. Couvreur, *Nat. Mater.* 2013, **12**, 991.

[33] P. Wust, B. Hildebrandt, G. Sreenivasa, B. Rau, J. Gellermann, H. Riess, R. Felix, P. M. Schlag, *Lancet Oncol.* 2002, **3**, 487.

[34] J. Pérez-Juste, I. Pastoriza-Santos, L. M. Liz-Marzán, P. Mulvaney, *Coord. Chem. Rev.* 2005, **249**, 1870.

[35] H. H. Richardson, Z. N. Hickman, A. O. Govorov, A. C. Thomas, W. Zhang, M. E. Kordesch, *Nano Lett.* 2006, **6**, 783.

[36] A. Ambrosone, P. D. Pino, V. Marchesano, W. J. Parak, J. M. de la Fuente, C. Tortiglione, *Nanomedicine* 2014, **9**, 1913.

[37] G. Gallot, D. Grischkowsky, *J. Opt. Soc. Am. B* 1999, **16**, 1204.

[38] D. Grischkowsky, S. Keiding, M. van Exter, C. Fattinger, *J. Opt. Soc. Am. B* 1990, **7**, 2006.

[39] E. C. Dreaden, A. M. Alkilany, X. Huang, C. J. Murphy, M. A. El-Sayed, *Chem. Soc. Rev.* 2012, **41**, 2740.

[40] A. O. Govorov, W. Zhang, T. Skeini, H. Richardson, J. Lee, N. A. Kotov, *Nanoscale Res. Lett.* 2006, **1**, 84.

[41] H. H. Richardson, M. T. Carlson, P. J. Tandler, P. Hernandez, A. O. Govorov, *Nano Lett.* 2009, **9**, 1139.

[42] G. O. Curme, F. Johnston, *Glycols*, Reinhold, New York 1953.

[43] A. Llevot, D. Astruc, *Chem. Soc. Rev.* 2012, **41**, 242.